Aggregation in organic phases after solvent extraction of uranyl nitrate: X-ray scattering and molecular dynamic simulations

Amaury Paquet, Olivier Diat, Laurence Berthon, Philippe Guilbaud

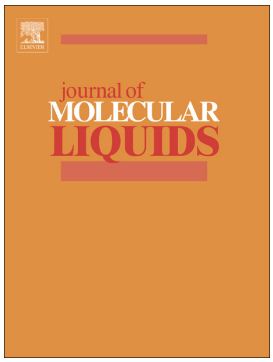

Aggregation in organic phases after solvent extraction of uranyl nitrate: X-ray scattering and molecular dynamic simulations

Amaury Paquet, Olivier Diat, Laurence Berthon, Philippe Guilbaud

PII: S0167-7322(18)34942-0
DOI: https://doi.org/10.1016/j.molliq.2018.12.051
Reference: MOLLIQ 10127

To appear in: *Journal of Molecular Liquids*

Received date: 25 September 2018
Revised date: 4 December 2018
Accepted date: 8 December 2018

Please cite this article as: Amaury Paquet, Olivier Diat, Laurence Berthon, Philippe Guilbaud , Aggregation in organic phases after solvent extraction of uranyl nitrate: X-ray scattering and molecular dynamic simulations. Molliq (2018), https://doi.org/10.1016/j.molliq.2018.12.051

Aggregation in Organic Phases after Solvent Extraction of Uranyl Nitrate: X-ray Scattering and Molecular Dynamic Simulations

Amaury Paquet[a], Olivier Diat[b], Laurence Berthon[a*] and Philippe Guilbaud[a*]

[a] CEA, Nuclear Energy Division, Reasearch Department on Mining and Fuel Recycling Processes (SPDS/LILA) BP17171 30207 Bagnols-sur-Cèze (France)

[b] ICSM,CEA,CNRS,ENSCM, Univ. Montpellier, BP17171 30206 Bagnols sur-Cèze (France)

[*] Corresponding authors: philippe.guilbaud@cea.fr ; laurence.berthon@cea.fr

Declarations of interest : none

ABSTRACT

In the framework of spent nuclear fuel reprocessing, N,N-dialkylamides are molecules of interest for the selective recovery of uranium and plutonium. Two monoamides, DEHBA (N,N-di-2-ethylhexyl-butyramide) and MOEHA (N,N-methyl, octyl-2-ethylhexanamide), were investigated to evaluate the effect of their structure on the molecular and supramolecular speciation in organic phase. The structure of the organic phases after water and uranyl nitrate extraction was characterized by combining experimental SWAXS with molecular dynamic simulations. After water extraction, N,N-dialkylamides solutions are mainly composed of monomers and dimers. In the case of MOEHA solutions, dimers and bigger aggregates containing 3 to 5 ligands molecules surrounding nano-cluster of water molecules are observed. The proportion of aggregates increases with the N,N-dialkylamide concentration. After extraction of high uranyl nitrate concentration, 0.5 mol·L^{-1} N,N-dialkylamide solutions in *n*-heptane are composed of large and dense aggregates of uranyl cations linked together by bridging nitrates and solvated by the monoamide. For 1.5 mol·L^{-1} N,N-dialkylamide solutions, the organization is quite different with the presence of a multitude of smaller aggregates. This study validates the approach coupling MD simulation and SWAXS to study the complexity of extractant organic phases.

Keywords: solvent extraction; organic phase; aggregation; N,N-dialkylamides; uranyl; molecular dynamic simulation; SWAXS

1. INTRODUCTION

The recycling of uranium and plutonium is currently performed at the industrial scale with the PUREX (Plutonium Uranium Refining by EXtraction) process based on solvent extraction separations using Tri-*n*-butylphosphate (TBP). However, the evolution of fuel and economic issues justify the studies of alternative processes and/or extractants. Among the various extractants investigated, the N,N-dialkylamides are promising. Studied since the 1960's [1], these reagents have shown excellent capacities to extract actinides (IV) and (VI) nitrates [2, 3]. Some advantages over TBP include generation of low impact radiolysis products and the elimination of the phosphorus atom [4-8]. Indeed, they are composed of only C, H, O and N and are completely incinerable, decreasing secondary waste volumes. Another advantage N,N-dialkylamides have is their tunable selectivity. Due to their synthetic ease [2, 9], modifications can be made on the side chains of the nitrogen as well as the alkyl chain linked to the C=O group to either increase or decrease their selectivity for a particular cation, *i.e* selectivity for hexavalent versus tetravalent ions [1, 3, 10-17]. The extraction of uranyl nitrate by N,N-dialkylamides has been described by a solvation mechanism, represented by the following equation where L represents the monoamide [10-15, 18] :

$$UO_2^{2+}{}_{(aq)} + 2NO_3^-{}_{(aq)} + 2L_{(org)} \rightarrow UO_2(NO_3)_2L_{2(org)}$$

Numerous studies have been performed with tracer levels of uranium using the classical slope analysis method [1, 11, 15, 19]. Under these experimental conditions, the variation of the log uranium distribution ratio as a function of the log N,N-dialkylamide concentration gives the solvation number (number of ligand involved in the metallic complex). A number of 2.0 is obtained at low extractant concentrations (lower than 0.2 $mol.L^{-1}$ in alkane) whereas a non

integer number (≈2.5) is obtained for higher extractant concentrations; the deviation being interpreted as non-ideal behavior due to interactions between free ligand and the metallic complexes [15, 20]. Under higher metal loading, the solvation number can be obtained by saturation of the ligand with the metallic cation using a salting out agent such as lithium nitrate [15, 20]. In these conditions, the ratio of ligand concentration over metal concentration in organic phase produces a stoichiometry of 2. However, these methods give only an average stoichiometric number. At low acidity, the characterization of uranyl nitrate - N,N-dialkyl amide complex by IR, UV-visible and X-ray absorption spectroscopy indicates the coordination of the metal cation with the amidic carbonyl group and with the nitrate ions in a bi-dentate mode [15, 21] . These characterizations are consistent with the crystallized forms of uranyl-nitrate-amide compounds in which the uranium is hexacoordinate in the equatorial plane with two bidentate nitrates and two oxygen amides [22, 23].

N,N-dialkylamide solutions in alkane were also characterized after solute extraction at supramolecular scale by vapor pressure osmometry and small angle X-ray or neutron scattering [24-26]. It has been shown that the extraction of different solutes promotes the aggregation in this order water < nitric acid < uranyl nitrate. After uranyl nitrate extraction, new species are formed, including the formation of well-ordered aggregates [24, 25]. Nevertheless, it is difficult to determine the structure of these solutions with only experimental tools. In order to solve this issue, an approach combining experimental studies with molecular dynamic (MD) simulations has been developed and applied to several extractant systems [26-28]. The coupling of MD simulations with experimental techniques is an efficient way to investigate the organic solutions of extractants which have weak tensioactive properties (high critical aggregation concentration, low aggregation number). In this approach, the composition of the organic solution is determined experimentally and used to build simulation boxes with precisely the same composition as the experimental solutions; this is the only experimental input of the MD

simulations. After equilibration of the simulated organic phase, the representativeness of the simulations is checked by comparing experimental data (densities and both small and wide angle X-ray scattered intensities) with the calculated ones.

N,N-2-ethylhexyl isobutyramide (DEHiBA) diluted in alkanes has been previously investigated at the molecular and supramolecular scale by combining experiment and theoretical calculations. It has been shown that for high uranium concentrations, taking into account only the formation of the monometallic complex $UO_2(NO_3)_2L_2$ is not sufficient [24, 27] and that an unexpected organization of the organic solution beyond the molecular scale occurs with the important role of nitrates acting as bridging ligands.

Studies on extraction behavior have shown that the extraction properties of N,N-dialkyl amides depend on their structure. The molecular organization of a few N,N-dialkyl amides solutions [24-27] have been investigated but to our knowledge no data has been reported on the influence of the structure of the N,N-dialkyl amide on the supramolecular organization.

This paper aims to provide a better understanding of (i) the effect of the chemical structure of the monoamides and (ii) the effect of high concentrations of solutes on the supramolecular organization and the physicochemical properties of the organic solution. The N,N-dialkylamides solutions were investigated after water and uranyl nitrate extraction. The two N,N-dialkylamides extractants chosen are N,N di-2-ethylhexyl-butyramide (DEHBA) and N,N methyl, octyl-2-ethylhexanamide (MOEHA) (Fig 1). The results will be compared to previous results from the investigation of DEHiBA [24, 26, 27] and to recent studies on the TBP molecule [28, 29].

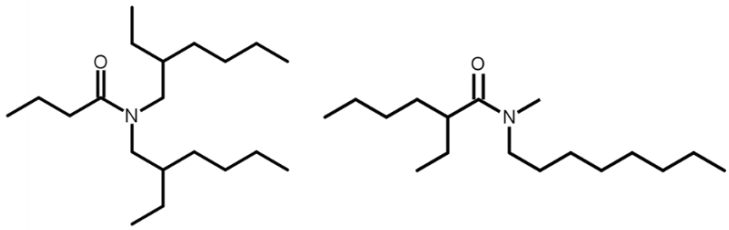

Fig 1 : Structure of the DEHBA (middle) and MOEHA (right) molecules

2. EXPERIMENTS AND METHODS

2.1. Materials

DEHBA and MOEHA were synthesized by Pharmasynthese (Lisses, France, purity ≥ 99%). *n*-Heptane was used as the diluent without further purification (Sigma Aldrich, purity ≥ 99%). The organic phases were prepared by dissolving weighed amounts of monoamide in *n*-heptane.

The 0.5 mol·L^{-1} U(VI) aqueous phase was prepared by dissolution of solid uranium (VI) nitrate hexahydrate ($UO_2(NO_3)_2.6H_2O$) obtained from Prolabo (purity > 99%) into a solution of 3 mol·L^{-1} lithium nitrate (reagent grade) with deionized water produced by the Milli-Q Plus apparatus (Millipore). The pH was adjusted to pH = 2 by adding a suitable volume of 1 mol·L^{-1} nitric acid.

2.2. Extraction

2.2.1. Water extraction

Organic solutions were contacted with deionized water with a V_{org}/V_{aq} volume ratio of 1:1. Extractions were performed at room temperature (~25°C) with 30 minutes stirring then aqueous and organic phases were separated after centrifugation.

2.2.2. Uranyl nitrate extraction

Extractions were carried out by contacting suitable volumes of an aqueous phase with organic phases in order to reach the targeted U(VI) concentration in the organic phases. The V_{org}/V_{aq}

volume ratios used in uranyl nitrate extraction experiments are summarized in Table 1. Extractions were performed at room temperature (~25°C) with 30 minutes stirring. Then aqueous and organic phases were separated after centrifugation.

Table 1 : Composition of aqueous and organic phases and volume ratios used for the extraction experiments

Solution	Initial Aqueous phase	Initial Organic phase	V_{org}/V_{aq}
DEHBA 0.5M – U 0.12M	$UO_2(NO_3)_2$ 0.5M $LiNO_3$ 3M HNO_3 10^{-2}M	DEHBA 0.5M in heptane	3/1
DEHBA 0.5M – U 0.22M			1/2
DEHBA 1.5M – U 0.40M		DEHBA 1.5M in heptane	1/1
MOEHA 0.5M – U 0.15M		MOEHA 0.5M in heptane	1/1
MOEHA 0.5M – U 0.19M			1/1.6
MOEHA 1.5M – U 0.45M		MOEHA 1.5M in heptane	1/1.4

2.3. Titration of solutes in organic solution

2.3.1. Water concentration

To determine the equilibrium concentration of water in each organic phase, Karl Fischer titrations were performed on a Metrohm 831KF coulometer with a range of detection between 10 μg and 10 mg of water. The reliability of the method was checked by the measurement of water content in a standard sample (Hydranal – Water standard 1.0 from Riedel de Haëns). The titrations were performed at least in triplicate to provide an estimated uncertainty of less than ± 5 %.

2.3.2. Uranium concentration

After extraction in the organic phase, uranyl nitrate was stripped by a 0.01 $mol \cdot L^{-1}$ nitric acid aqueous phase (1:100 organic/aqueous phase volume ratio). Then, after 30 minutes of stirring and centrifugation, aqueous solutions were diluted in 1 $mol \cdot L^{-1}$ nitric acid for X-ray

fluorescence titration (Thermo Scientific - ARL QUANT'X – EDRXRF Analyser). The calibration range, performed with references solutions of uranyl nitrate was 0-1000 $mg.L^{-1}$.

2.4. Density measurement

The densities of organic solutions after extraction were determined at 25°C using a Anton Paar – Stabinger (SVM 3000) densitometer with a resolution of $\pm 1 \times 10^{-5}$ $g{\cdot}cm^{-3}$.

2.5. Small and wide-angle X-ray scattering

Small and wide-angle X-ray scattering (SWAXS) experiments were carried out on a bench scale instrument built by Xenocs and using Mo radiation (λ = 0.71 Å). Thanks to off-center detection, a large q range was covered ($0.03\ Å^{-1} < q < 3\ Å^{-1}$). The value q is defined as:

$$q = \frac{4\pi}{\lambda} \times \sin\left(\frac{\theta}{2}\right)$$

Where θ is the X-ray scattering angle. Collimation was applied using a 12:∞ multilayer Xenocs mirror coupled to two sets of Forvis scatterless slits providing a 0.8 mm x 0.8 mm X-ray beam at the sample position.

Quartz capillaries (2 mm in diameter) containing the samples were used. The experimental resolution is $\Delta q/q = 0.05$. Absolute intensities in cm^{-1} were obtained using a 2.36-mm-thick high-density polyethylene sample (Goodfellow®) as a calibration standard.

Data pre-analysis was performed using FIT2D software, which takes into account the electronic background of the detector, transmission measurements (using a photodiode that can be inserted upstream the sample) and empty cell subtraction. Due to the use of Mo radiation (17.45 keV) with uranyl compounds, undesired fluorescence due to the uranium L-edge X-ray absorption is generated and increases the background intensity. The fluorescence background subtraction (a constant value versus q) was determined by SWAXS intensities of a same concentration monoamide organic solution without uranium. The subtraction value was the difference

between the maximum intensity of peak at 1.42 $Å^{-1}$ (aliphatic chains first shell in the solution) of the solution without uranium and the same with uranium fluoresence. Then intensities are normalized (maximum of peak at 1.42 $Å^{-1}$ set to 1) for comparison.

2.6. Molecular dynamic (MD) simulations

For each solution, molar ratios of all components were calculated from experimental data in order to build boxes with the exact same composition as experimental solutions. Then simulation boxes were built using the Packmol package [30]. For simulation of solutions without uranyl nitrate and for solution with 0.5 $mol·L^{-1}$ monoamide with uranyl nitrate, the molecules were randomly distributed at starting point. For simulations of 1.5 $mol·L^{-1}$ monoamide solutions with uranyl nitrate, $UO_2(NO_3)_2L_2$ complexes were pre-formed (with two bidentate nitrate ions and two monoamide ligands directly linked to each uranyl cation –similar to structure on top of Fig 10 or Fig 12) then distributed randomly in the simulation boxes with the other constituents.

MD simulations were performed using the AMBER 14 [31] software with the parm99 force field [32, 33] and taking into account explicitly polarization effects which are essential for a good representation of the dispersion forces and polarization interactions [34]. Atomic partial charges on DEHBA, MOEHA and *n*-heptane were calculated with the restricted electrostatic potential procedure [35, 36] (Supporting info S1). Water molecules were described using the POL3 model [37]. The UO_2^{2+} cation Lennard-Jones parameters were adjusted in previous study [38] in order to take into account the explicit polarization effects on its first hydration shell geometry. Equations of motion were numerically integrated using a 1 fs time step. MD simulations were performed using periodic boundary conditions with a 15 Å truncation cut-off and long range interactions were calculated using the particle-mesh Ewald method [39]. Temperature was set at 298 K. Boxes were equilibrated for at least 2 ns in the NPT ensemble. MD simulations were collected for at least 5 ns for simulations of water extraction and at least

10 ns for simulations of uranyl nitrate extraction. Radial distribution functions and snapshots were obtained using the VMD 1.9.2 software [40]. Structure factors of the simulated boxes were computed using nMoldyn [41]. Static coherent structure factor were calculated over a range of 0-3 $Å^{-1}$ with a step of 0.01 $Å^{-1}$.

3. RESULTS AND DISCUSSION

3.1. Water extraction

3.1.1. Organic phase composition analyses

After contacting the organic phase of DEHBA and MOEHA (0.5 to 2 $mol.L^{-1}$) in *n*-heptane with pure water and separating the phases, the organic phase densities were experimentally measured, and the water concentrations were quantified (Table 2).

An increase of the water concentration in the organic phase is observed with the increase the extractant concentration but the $[H_2O]_{(org)}/[L]_{(org)}$ ratio remains quite low (< 0.13) even for the more concentrated solutions. These concentrations are in the same order of magnitude and are comparable to what was observed for organic phases containing DEHiBA [24] extractant but, they are much lower than the literature values for malonamide[42, 43] or TBP [28, 44, 45] extractants. On the other hand, organic solutions of 0.5 $mol.L^{-1}$ of DEHiBA in *n*-heptane after water extraction seem to have ideal behavior whereas small aggregates in alkane diluents are observed for malonamide and TBP solutions which solubilize water molecules. The water concentration seems to be correlated with the aggregation states of the solutions.

The comparison of the DEHBA and MOEHA solutions indicates that the extracted water concentration for MOEHA solutions are slightly higher than for DEHBA solutions (about 1.4 times less water extracted for the latter).

Table 2 : Composition of solutions of DEHBA and MOEHA considered for MD simulations. Calculated and experimental densities in are g.cm^{-3} at 25°C. L is the ligand.

	Experiment			MD simulations				
	Concentration (mol·L^{-1})		ρ_{exp}	ρ_{calc}	Number of molecules			Box size (Å)
	L	H_2O			heptane	L	H_2O	(x/y/z)
DEHBA	0.5	0.013	0.715	0.709	1500	137	4	77/77/77
	1.0	0.059	0.754	0.749	1035	241	14	78/73/69
	1.5	0.096	0.783	0.778	1035	507	32	82/82/82
	2.0	0.187	0.819	0.817	1035	1090	102	98/97/95
MOEHA	0.5	0.030	0.709	0.705	1500	127	8	76/76/76
	1.0	0.079	0.742	0.742	2000	434	34	89/89/89
	1.5	0.152	0.769	0.767	1200	521	56	83/83/83
	2.0	0.246	0.799	0.797	2000	1576	194	109/109/109

3.1.2. SWAXS experiments

To obtain a comprehensive analysis of the organization of the solutions at both the molecular and supramolecular scales, small and wide-angle X-ray scattering experiments were performed on the organic solutions (Fig 2). The shape of the experimental scattering intensity (Fig 2- left) depends on the monoamide concentration in the samples. This reflects a change of organization with the extractant concentration in the organic solution. The peak at 1.42 Å^{-1} is common to all the scattering curves and can be related to the aliphatic chains inter-distances [26, 27]. For the concentrations of DEHBA above 1 mol·L^{-1}, a correlation peak appears around 0.7 Å^{-1} that, increases in intensity and does not shift with the extractant concentration. This peak can be attributed to a correlation distance between the polar parts of the monoamides similar as what can be encountered in the pure solution of monoamide. This is a usual observation in polar organic solvents and this correlation distance is known to scale with the aliphatic size of the molecule [27, 28, 46, 47]. Considering MOEHA, a similar correlation peak appears, but at lower q-values and at higher ligand concentration (above 1.5 mol·L^{-1}). However, its intensity is much lower, a sign of a poorly defined correlation distance between the polar amide heads. The last point is that contrary to diamide systems[43, 48-53] under similar conditions, no scattering

upturn at small q values was observed, indicating no formation of large compact aggregates that could create a significant electronic density fluctuation detectable by SWAXS.

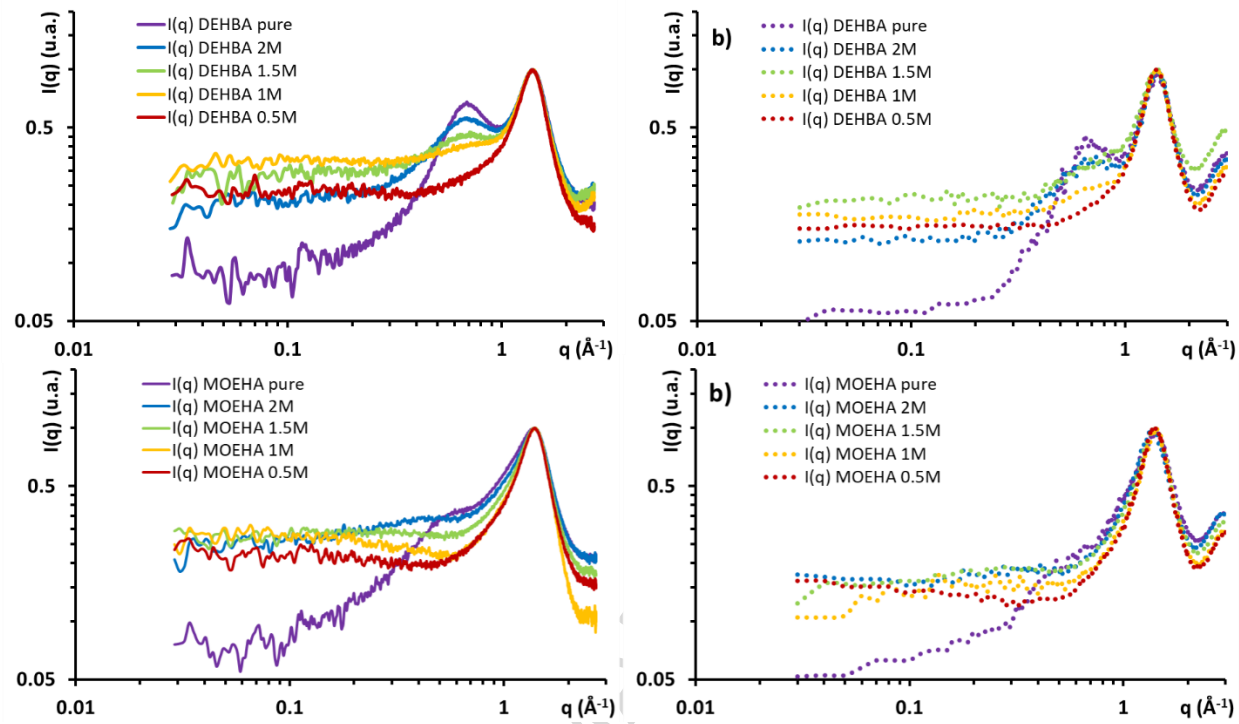

Fig 2 : Experimental (left) and calculated (right) SWAXS intensities for DEHBA (up) and MOEHA (down) in *n*-heptane (room temperature) after water extraction with increasing extractant concentration

3.1.3. MD simulations

MD simulation boxes were built and equilibrated with the molecule amounts determined experimentally (Table 2), and theoretical SWAXS intensities were calculated from the MD trajectories for each solution (Fig 2 – right) following the procedure described in reference [27]. The calculated SWAXS intensities profiles are in good agreement with the experimental ones. The I(q) peak at 1.42 $Å^{-1}$ is well reproduced. The position of the second correlation peak (0.3 or 0.7 $Å^{-1}$) is also well reproduced for both monoamides, as well as its increase of intensity with the increase of the extractant concentration. This agreement between experimental and calculated SWAXS intensities supports the representativeness of the simulated solutions.

In order to describe and quantify the nature of the interactions present in the organic solutions, the radial distribution functions (RDF) were computed to gather average intermolecular

distances between oxygen atoms (amide oxygen atoms and water oxygen atoms). For each RDF, the distance corresponding to the peak maximum and the number of atoms calculated from the integration of the RDF peak are reported in Table 3. For example, the RDF of amide oxygen atoms centered on amide oxygen atoms (RDF $O_{c=o}$, $O_{c=o}$) are reported in Fig 3. Additional RDFs are reported in the supporting info (Fig. S3 to Fig. S10). The RDF are very noisy for the 0.5 mol·L^{-1} simulations since (i) the number of ligands in the simulation boxes is low and (ii) the formation of aggregates is very unlikely at this extractant concentration. For these simulations, the positions of the peaks and the cut-off distances for their integrations have therefore been selected from the highest extractant concentration RDFs.

Table 3 : Average atom coordination environment calculated from RDF. $O_{c=o}$ is monoamide oxygen atom and O_{wat} is water oxygen atom. First atom in brackets is the center atom of the RDF. N corresponds to the number of atoms (integration of the corresponding peak).

	[L]	[H_2O]	peak	($O_{c=o}$, $O_{c=o}$)		($O_{c=o}$, O_{wat})		(O_{wat}, O_{wat})	
				d (Å)	N	d (Å)	N	d (Å)	N
DEHBA	0.5	0.013	**1st**	3.6	0.05	2.8	0.02	-	-
			2nd	-	-	-	-	-	-
	1.0	0.059	**1st**	3.6	0.08	2.8	0.05	2.8	0.2
			2nd	-	-	-	-	-	-
	1.5	0.096	**1st**	3.6	0.08	2.8	0.05	2.8	0.7
			2nd	5.7	0.5	-	-	-	-
	2.0	0.187	**1st**	3.6	0.1	2.8	0.08	2.8	1.2
			2nd	5.7	0.6	5.0	0.08	-	-
MOEHA	0.5	0.030	**1st**	6.4	0.5	2.8	0.05	2.8	0.4
			2nd	-	-	-	-	-	-
	1.0	0.079	**1st**	6.4	0.9	2.8	0.07	2.8	0.4
			2nd	-	-	-	-	-	-
	1.5	0.152	**1st**	6.4	1.4	2.8	0.1	2.8	0.7
			2nd	-	-	-	-	-	-
	2.0	0.246	**1st**	6.4	2.0	2.8	0.1	2.8	1.5
			2nd	-	-	5.0	0.15	-	-

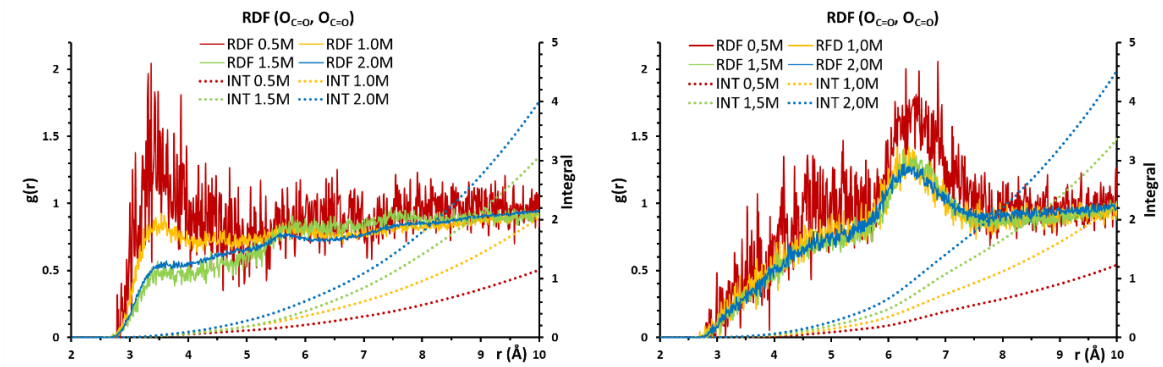

Fig 3 : Radial distribution functions and integration of amide oxygen atoms versus amide oxygen atoms for DEHBA (left) and MOEHA (right) simulations. Left axis corresponds to RDFs (solid lines), right axis corresponds to integrals (dotted lines).

For all concentrations of DEHBA, a broad peak is observed at a quite short distance (3.6 Å) indicating DEHBA molecules interacting with each other. The integration of this peak accounts for a small amount of DEHBA (less than 10%) interacting at this short distance. There is a slight increase (from 5 to 10%) of extractant molecules interacting with each other when the extractant concentration increases from 0.5 to 2 mol·L^{-1}. A visual analysis of the MD simulations shows that this short correlation distance corresponds to the formation of monoamide dimers, which is in agreement with what has been previously observed for DEHiBA extractants [26]. At high DEHBA concentration (above 1.5 mol·L^{-1}), a second broad peak appears around 5.7 Å, indicating correlation of the extractant at a slightly larger scale.

The number of water molecules interacting with a carbonyl oxygen atom also increases with the organic water concentration (from 0.02 to 0.08), and the probability for a water molecule to have another water molecule in its first sphere increases with the increase of both ligand and water concentration. This means that the increase of the concentration of DEHBA leads to the formation of aggregates larger than dimers observed at low extractant concentration, with water molecules included in these aggregates. In order to quantify the percentage of DEHBA molecules in monomeric form or aggregated in each solution, the number of DEHBA molecule in "contact" with other DEHBA molecule within a range of 4 Å (end of the first RDF peak) and 6 Å (end of the second RDF peak) was computed. The analysis for a 4 Å radius shows the

presence of short distance dimers which are bonded by dipole-dipole interactions, and the analysis for a 6 Å radius highlights the formation of larger species. Percentages of each species for each simulation are reported in Table 4.

Table 4 : Percentage of monoamide molecules involved in the different species. Short distance dimers are molecules in dipole-dipole interaction and long distance dimers are molecules in interaction through water molecule.

	Concentration ($mol \cdot L^{-1}$)	Monomer	Short distance dimer	Long distance dimer	Trimer	tetramer	pentamer
DEHBA	0.5	90 %	5 %	5 %	0 %	0 %	0 %
	1	61 %	8 %	26 %	5 %	0 %	0 %
	1.5	53 %	7 %	31 %	8 %	1 %	0 %
	2	42 %	4 %	40 %	13 %	1 %	0 %
MOEHA	0.5	93 %	/	7 %	0 %	0 %	0 %
	1	42 %	/	39 %	15 %	4 %	0 %
	1.5	27 %	/	39 %	24 %	9 %	1 %
	2	30 %	/	34 %	23 %	10 %	3 %

The percentage of short distance dimers is low, under 8% for all solutions. At the lowest DEHBA concentration ($0.5\ mol \cdot L^{-1}$), there are mainly monomers (90%), 5% of the monoamides are involved in short distance dimers and the last 5% are involved in long distance dimers. These long-distance dimers are bonded by one or several water molecules.

For the higher DEHBA concentrations, the proportion of monomers drops drastically from 61% for [DEHBA] = $1\ mol \cdot L^{-1}$ to 42% for the highest concentrated solution. Concurrently, the proportion of long distance dimers increases from 26% to 40% and some larger aggregates are formed (5 to 13% of trimers and less than 1% of tetramers). The increase extractant concentration leads to an increase of long distance interactions between monoamides. This results in the appearance of a peak in the SWAXS data around $0.7\ Å^{-1}$ increasing with the extractant concentration.

In all cases, the interactions occurring between DEHBA molecules are weak, as indicated by the broad correlation peaks on the $O_{c=o}$, $O_{c=o}$ RDFs in Fig 3. This can be illustrated by the snapshots shown in Fig 4 that show the distribution of monoamide aggregates in the simulation boxes for the different monoamide concentrations. Monoamides highlighted in purple are in interaction within a distance of 4 Å (first peak of the RDF $O_{c=o}$, $O_{c=o}$) and those highlighted in green are in interaction within a distance of 6 Å (second peak of the RDF). The predominant types of aggregates observed in the simulation boxes from [DEHBA] = 1 mol·L^{-1} are dimers with dipole-dipole interaction or interactions with water molecules (Fig 5).

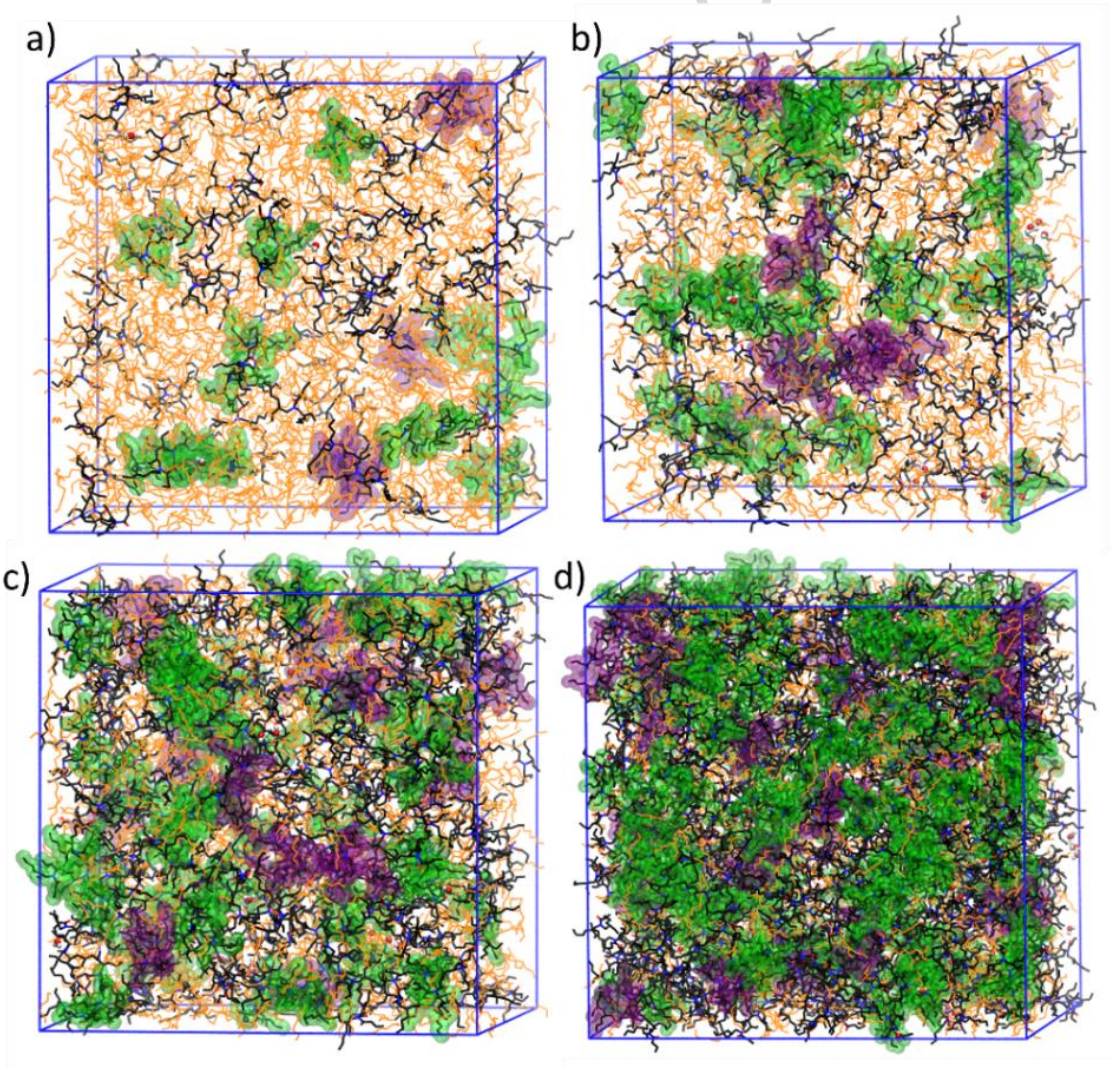

Fig 4 : Snapshots of simulations boxes of DEHBA solutions, a) 0.5 mol·L^{-1}, b) 1.0 mol·L^{-1}, c) 1.5 mol·L^{-1} and d) 2.0 mol·L^{-1}. Heptane are in orange, carbon in black, nitrogen in blue and oxygen in red. DEHBA molecules highlighted in purple are in interaction within 4 Å (first peak of the RDF Oc=o, Oc=o). Molecules highlighted in green are in interaction within 6 Å (second peak of the RDF Oc=o, Oc=o).

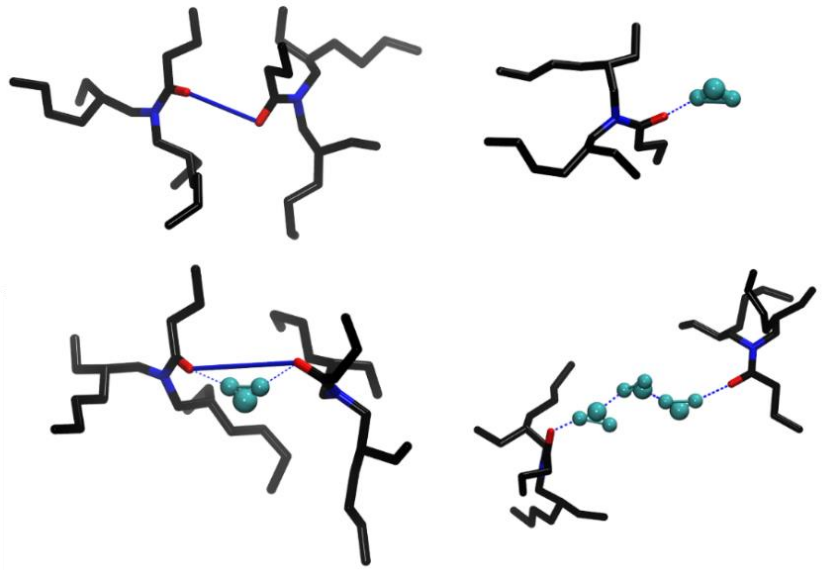

Fig 5 *:* Representative structures of the predominant aggregates observed in DEHBA simulation boxes. Straight blue lines: dipole-dipole interactions, dotted blue lines: hydrogen bonds, water molecules are in light blue.

The organization of the organic phase containing MOEHA is quite different. First, the highest probability of finding an amide oxygen atom in proximity of another one is found at a distance of 6.4 Å (the first $O_{C=O}$,$O_{C=O}$ RDF peak), *i.e.* a much longer distance than in the case of DEHBA (Fig 3). Below 6.4 Å, the intensity of the RDF slightly increases, but without any correlation peaks, indicating that some short distance interactions between MOEHA extractants may occur, but in the fast kinetic exchange region. The number of MOEHAs located within 4 Å of each other (characteristic distance for monoamide short distance dimer formation) was calculated to account for the number of extractants interacting at this short distance. Even for the highest extractant concentrations, less than 3% of MOEHA is dimerized. The increase in the concentration of MOEHA leads to the increase of the number of MOEHAs located at the longer 6.4 Å equilibrium distance (from 0.5 to 2.0). These two features, very low number of MOEHA involved in correlation at less than 4 Å, and more at higher distance (around 6.4 Å), indicate that these monoamide extractants form preferentially larger structures than DEHBA. This is strengthened by the slightly increased amount of water interactions with each other for all MOEHA extractant concentrations (from 0.4 to 1.5). The percentage of MOEHA molecules involved in each species was calculated for a radius of 7.5 Å (end of RDF peak) and the results

are presented in Table 4. In the less concentrated solutions, monomers are predominant (93%) like for DEHBA. However above [MOEHA] = 1 mol·L^{-1} the percentage of monomers decreases more than with of DEHBA, and almost no short distance dimers are formed. Long distance dimers are the predominant species (34 to 39%) and MOEHA molecules also aggregate into larger species in a non-negligible amount such as trimers (15 to 24%), tetramers (4 to 10%) and pentamers (less than 3%) for the most concentrated solutions.

These results can be visualized in Fig 6, where aggregates within a distance of 4 Å (purple) and within a distance of 7.5 Å (green) are highlighted. As a result, we observe that the quantity of short distance dimers is very low while large aggregates are common. Furthermore, the observation of the predominant aggregates in the MD boxes shows that these aggregates are formed with 2 to 5 MOEHA molecules surrounding nano-droplets of water molecules (Fig 7).

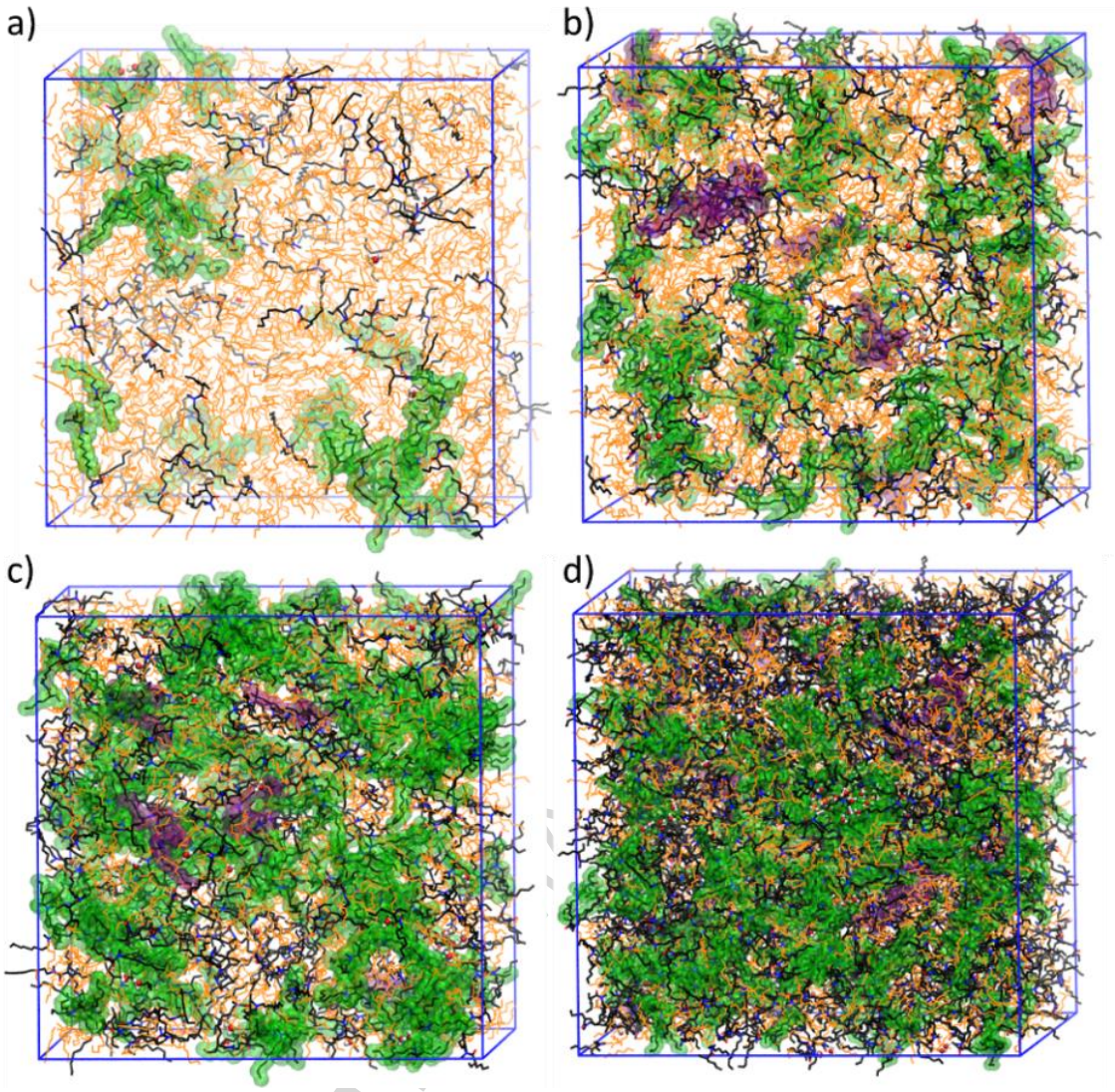

Fig 6 *:* Snapshots of simulations boxes of MOEHA solutions, a) 0.5 mol·L^{-1}, b) 1.0 mol·L^{-1}, c) 1.5 mol·L^{-1} and d) 2.0 mol·L^{-1}. Heptane are in orange, carbon in black, nitrogen in blue and oxygen in red. MOEHA molecules highlighted in purple are interacting within 4 Å (first peak of the RDF Oc=o, Oc=o). Molecules highlighted in green are interacting within 7.5 Å (second peak of the RDF Oc=o, Oc=o).

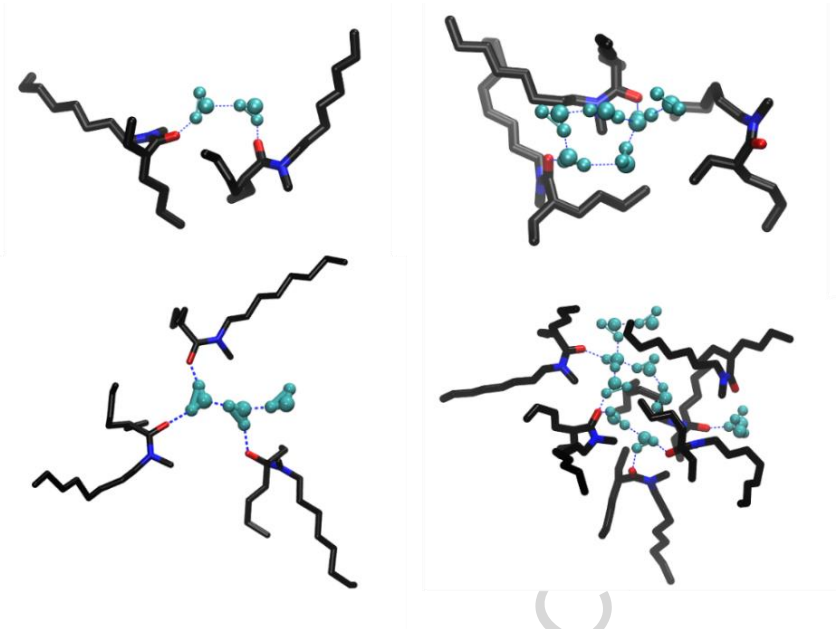

Fig 7 : Representative structures of the predominant aggregates observed in MOEHA simulation boxes. Dotted blue lines: hydrogen bonds, water molecules in light blue

From this data and the previous data obtained with DEHiBA solution in *n*-heptane [27], it seems that the change in the N,N-dialkylamide structure (branched vs. linear alkyl chain) affects the aggregation state of the solution and the water extraction. The presence of a branched chain near the amide function seems to inhibit the formation of long-range correlations between the extractants. For example for a 1 mol·L^{-1} of N,N-dialkyl amide solution in *n*-heptane, 82 % ; 61% and 63 % of monomers are present for DEHiBA ; DEHBA and MOEHA respectively. Therefore, on one side, the ramification close to the C=O group of the amide function has a strong impact on the monomer concentration, and on the other side, the amount of water extracted in the organic phase has a strong impact on the shape of the aggregates (for MOEHA phases that contain twice more water than DEHBA phases, long range dimers and bigger aggregates are preferentially formed).

Nevertheless, the organization of the N,N-dialkyl amide solutions after water extraction is quite different from those of the TBP or malonamide solutions. After water extraction, N,N-dialkylamide solutions in *n*-heptane are composed mainly of monomers (40-60% for solutions at 1 mol.L^{-1}) and dimers whereas TBP (1 mol.L^{-1}) or malonamide (0.6 mol.L^{-1}) solutions in *n*-

heptane are primarily organized into small aggregates composed of two to four molecules (reverse micelles type aggregate). Only 10% and 25% of monomers remain in the solution for TBP and malonamides respectively [27, 28]. The water concentration in the organic phase is dependent on the aggregation state of the solutions: less than 0.08 mol.L^{-1} of water is extracted with 1 mol.L^{-1} N,N-dialkylamide solution vs 0.42 and 0.18 mol.L^{-1} respectively for TBP (1 mol.L^{-1}) or malonamides (0.6 mol.L^{-1}) solutions in *n*-heptane [27, 28, 43].

3.2. Uranyl nitrate extraction

3.2.1. Organic phases composition analyses

Organic phases of DEHBA and MOEHA containing two different concentrations of monoamide (0.5 and 1.5 mol·L^{-1}) were contacted with a solution of uranyl nitrate in 3 mol·L^{-1} $LiNO_3$ at pH = 2. The experimental data for DEHBA and MOEHA solutions are reported in Table 5 with the corresponding number of molecules, boxes sizes and simulated solution densities at the equilibrium.

Table 5 : Composition of solutions of DEHBA and MOEHA considered for MD simulations. Calculated and experimental densities in g.cm^{-3} at 25°C. L is the ligand.

	Experiment				**Molecular dynamic**						
	Concentration (mol·L^{-1})			ρ_{exp}	ρ_{calc}	Number of molecules					Box size (Å)
	L	H_2O	UO_2			heptane	L	H_2O	UO_2	NO_3	(x/y/z)
DEHBA	0.5	0.02	0.12	0.770	0.753	2450	222	10	52	104	91/90/90
	0.5	0.02	0.22	0.799	0.787	2216	200	8	88	176	87/87/87
	1.5	0.08	0.40	0.943	0.909	1500	736	38	193	386	94/94/94
MOEHA	0.5	0.03	0.15	0.772	0.759	2000	175	11	52	104	84/84/84
	0.5	0.03	0.19	0.788	0.772	2000	175	11	66	132	84/84/84
	1.5	0.14	0.44	0.937	0.910	1800	754	70	222	444	95/95/95

3.2.2. SWAXS experiments

Similarly to the study of the extraction of water, SWAXS measurements were performed in order to investigate the structure of the solutions at the supramolecular scale. The two solutions of 0.5 mol·L^{-1} of DEHBA (Fig 8 – upper left) show a small angle scattering upturn with an

intensity that depends on the concentration of U(VI). This suggests the presence of large and dense aggregates. At 1.5 mol·L^{-1} of DEHBA, a broad correlation peak grows in around 0.5 Å^{-1} simultaneously as the decrease of the scattering at lower angles. This suggests either the presence of smaller aggregates with a more limited and defined range of sizes or, more likely a repulsive interaction between the aggregates formed at lower monoamide concentration due to their increase in number.

Regarding the MOEHA system (Fig 8 – lower left), a similar SWAXS curve evolution is observed with a less pronounced effect for the intermediate correlation peak, which is still correlated with the decrease of the scattering upturn at low q-values. The small peak at 0.4 Å^{-1} observed for the highest UO_2^{2+} concentration is due to the signals of the kapton window (used in the x-ray scattering optical path) that is difficult to subtract due to the strong fluorescence of uranium.

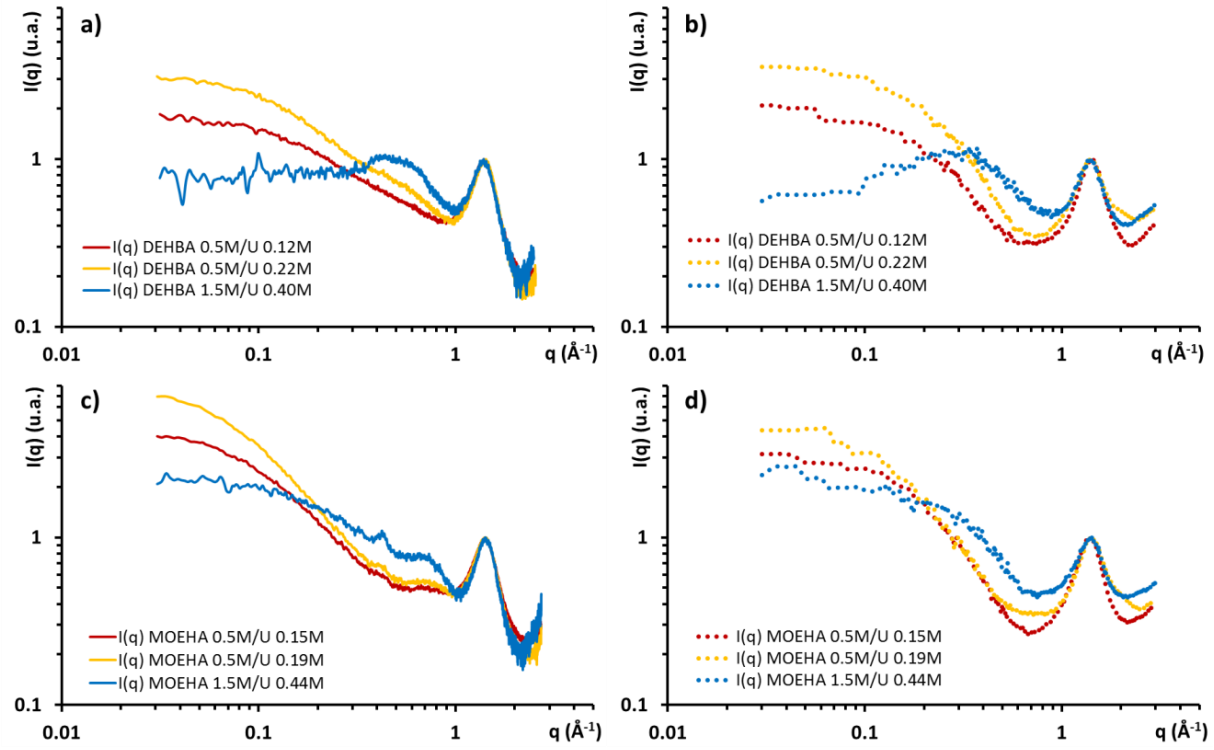

Fig 8 : Experimental (left) and calculated (right) SWAXS intensities for DEHBA (top) and MOEHA (bottom) 0.5 mol·L^{-1} and 1.5 mol·L^{-1} in *n*-heptane (room temperature) after extraction of uranyl nitrate.

3.2.3. MD Simulations

MD simulation boxes were built and equilibrated with the molecule amounts determined experimentally (Table 5). SWAXS intensities were calculated from MD trajectories for each solution (Fig 8 - right). Calculated intensities are in good agreement with the experimental ones. The peak corresponding to aliphatic chain interactions at 1.42 $Å^{-1}$ is well reproduced in all cases. The small angle intensity increasing for the solutions at 0.5 $mol{\cdot}L^{-1}$ is reproduced by the simulations. The shape change of the curves for the solutions at 1.5 $mol{\cdot}L^{-1}$ is also well reproduced. However, for the DEHBA solution, the broad peak is reproduced but centered at slightly lower value of q (around 0.35 $Å^{-1}$). This is certainly due to the fluorescence corrections done for the experimental intensities that depends slightly on the scattering angle in the geometry of analysis. Simulations of these more concentrated boxes were performed with $UO_2(NO_3)_2L_2$ complexes pre-formed at the starting point. Other starting points were tried for the simulations (no pre-formed complexes, artificial constraints on uranium and monoamides/nitrates distance) but they did not provide calculated SWAXS signal in agreement with the experimental ones (see Fig. S11 in supporting information). Considering the complexity of the simulated solutions, the results presented are more than satisfactory: the calculated SWAXS intensities are close to the experimental ones, without any artificial constraints used in the MD simulations.

Statistical analysis from RDFs were performed in order to describe the average environment of uranyl cations. RDFs centered on uranium atoms have been calculated for the distribution of amide oxygen atoms (U, $O_{C=O}$), water oxygen atoms (U, O_{wat}), all oxygen atoms (U,O_{tot}), nitrate nitrogen atoms (U, O_{nit}), and uranium atoms themselves (U, U). Results are reported in Table *6*.

Table 6 : Average atom coordination environment calculated from RDF. $O_{c=o}$ is monoamide oxygen atom and O_{wat} is water oxygen atom, N_{nit} is nitrate nitrogen. First atom in brackets is the center atom of the RDF.

	[L] (mol/L)	[UO_2] (mol/L)	peak	(U, $O_{c=o}$)		(U, O_{wat})		(U, N_{nit})		(U, U)		(U, O_{tot})	
				d (Å)	N	d (Å)	N	d (Å)	N	d (Å)	N	d (Å)	N
DEHBA	0.5	0.12	**1st**	2.43	0.7	2.43	0.2	2.79	0.7	5.83	1.7	2.40	5.1
			2nd	4.40	0.5	-	-	3.56	2.8	6.79	0.4	-	-
	0.5	0.22	**1st**	2.43	0.6	2.43	0.1	2.79	0.7	5.83	1.9	2.40	5.0
			2nd	4.40	0.5	-	-	3.56	3.0	6.79	0.8	-	-
	1.5	0.40	**1st**	2.43	1.4	2.43	0.1	2.79	1.4	5.83	0.6	2.40	5.5
			2nd	4.40	0.6	-	-	3.56	1.2	6.48	0.1	-	-
MOEHA	0.5	0.15	**1st**	2.43	0.7	2.43	0.2	2.79	0.6	5.83	1.6	2.40	5.0
			2nd	4.38	0.7	-	-	3.56	3.0	6.79	1.0	-	
	0.5	0.19	**1st**	2.43	0.6	2.43	0.2	2.79	0.5	5.83	2.0	2.40	5.0
			2nd	4.38	0.8	-	-	3.56	3.3	6.79	0.7	-	-
	1.5	0.44	**1st**	2.43	1.0	2.43	0.2	2.79	0.8	5.83	1.1	2.40	5.2
			2nd	4,38	0,7	-	-	3.56	2.4	6.68	0.4	-	-

First, (U, U) radial distribution functions were used to determine if polymetallic uranyl aggregates are formed in the organic phases (Supporting info Fig. S11 to Fig. S16). The presence of a clear peak at 5.83 Å on the (U,U) RDF indicates a preferential distance with a relevant probability between uranium atoms. Its integration gives information on the number N(U, U) of uranium atom "connected" at this preferential distance. An average number equal to 1 is characteristic of the formation of bimetallic aggregates (each uranium atom is connected to one and only one other uranium atom). An average N(U, U) equal to 1.3 is characteristic of the formation of trimetallic aggregates, etc. For both DEHBA and MOEHA extractants, the integration of this RDF peak is between 0.6 and 2.0. This indicates that depending on the concentration of extractant and uranium, different complexes or aggregates are formed in the organic phases, potentially from monometallic complexes to large aggregates including more than 3 uranyl cations.

In order to get insight into this complex speciation, the percentage of uranyl cations connected with each other was calculated by counting the number of uranyls located within a radius of 6.2 Å that corresponds to the end of the RDF (U, U) peak (results are reported in Table 7).

Table 7 : percentage of uranyl cation(s) having 0 to 4 connections with other uranyl cation in DEHBA and MOEHA organic phases within a 6.2 Å radius.

Number of U-U connections	0	1	2	3	4
DEHBA 0.5M – U 0.12M	15	42	26	16	1
DEHBA 0.5M – U 0.22M	10	32	38	16	3
DEHBA 1.5M – U 0.40M	57	37	6	0	0
MOEHA 0.5M – U 0.15M	14	42	29	13	2
MOEHA 0.5M – U 0.19M	9	27	34	25	4
MOEHA 1.5M – U 0.44M	22	52	23	3	0

In the literature, the uranyl nitrate complex formed after it's extracted by N,N-dialkyl amide is usually described as $UO_2(NO_3)_2L_2$. The two main approaches to obtain this 1:2 stoichiometry complex are usually slope analysis approach where trace level concentrations of uranium are used [1, 10-17, 19], or the saturation of the ligand with metallic cation [15, 20]. However, for [DEHBA] = 0.5 mol·L^{-1}, this $UO_2(NO_3)_2L_2$ species is a minority in the MD simulations: 15% and 10% of uranyl only are involved in this complex for $[UO_2^{2+}]$ = 0.12 and 0.22 mol·L^{-1} respectively. Polymetallic aggregates are predominant and their proportion increases with the uranium concentration. For $[UO_2^{2+}]$ = 0.12 mol·L^{-1}, 42% of the uranium atoms are connected to only one other uranium atom and 26% are connected to two other uranium atoms at an average distance of 5.83 Å. For $[UO_2^{2+}]$ = 0.22 mol·L^{-1}, the decrease of the monometallic complex proportion is correlated with the increase of higher order connections between uranium atoms: 32% of the uranium atoms are only connected to one other and 38% are connected with two other uranium atoms. This indicates that the size of the polymetallic uranium aggregates increases with the concentration of uranium in the organic phase. In these polymetallic aggregates, the uranyl cations are linked by bridging nitrates, the second peak of RDF(U, Nnit), which results in a decreasing amount of bidentate nitrate, the first peak of RDF(U, Nnit), in uranium's first coordination sphere. There is finally a decrease of the total coordination number of UO_2^{2+} to 5, which is consistent with the decrease number of bidentate nitrate ions in the uranyl first coordination sphere, as reported in previous studies [26-28]. The speciation is

confirmed by the other RDFs analyses: (i) the integration of the RDF (U, U) first peak increases from 1.7 to 1.9; (ii) the coordination number of U in the equatorial plane of UO_2^{2+}, given by RDF(U, O_{tot}) in Table 6, is close to 5; and (iii) the number of bidentate nitrate per uranyl cation, given by RDF(U, N_{nit}), is equal to 0.7 (much less than 2). The number of DEHBA extractants in the first coordination sphere of each uranyl cation is surprisingly low: less than one monoamide is directly bound to each uranium atom (0.7 or 0.6 for $[UO_2^{2+}] = 0.12$ and 0.22 mol·L^{-1}, respectively). This is, in part, counterbalanced by the presence of DEHBA in the uranium's second coordination sphere (0.5 monoamide in average for each UO_2^{2+}), but the average stoichiometry in these aggregates, between 1.2 and 1.1 at [DEHBA] = 0.5 mol·L^{-1} remains lower than in the diluted organic phases. In both solutions, there are few water molecules present. Theses water molecules are, for the most part, bonded to uranyl cations in the uranium's first coordination sphere.

In order to test the influence of the uranyl nitrate concentration on this speciation, an additional molecular dynamics simulation has been performed for [DEHBA] = 0.5 mol·L^{-1}, with a low uranyl nitrate concentrations ($[UO_2(NO_3)_2] = 0.03$ mol·L^{-1}). In this simulation, only the 1:2 complex with one uranyl cation surrounded by two monoamide extractants and two bidentate nitrates is formed (U coordination number = 6), in agreement with the slope analyses experiments performed in dilute uranyl organic phases.

At high extractant concentration ([DEHBA] = 1.5 mol·L^{-1}), the speciation is drastically different: 57% of the uranyl cations are involved in monometallic 1:2 complexes, 37% are connected with one cation and only 6 % are connected with two cations. The resulting average uranyl nitrate extracted species, contains 2 DEHBA (1.4 in the uranium first coordination sphere and 0.6 in its second coordination sphere) and 2.6 nitrate ions (1.4 bidentate and 1.2 bridging or monodentate nitrates).

This speciation of DEHBA organic phases (both for the 0.5 and 1.5 mol·L^{-1} solutions) is in agreement with the experimental and simulated SWAXS intensities that shows: (i) low q increase for the two solutions at 0.5 mol·L^{-1} of DEHBA which correspond to the large polymetallic aggregates, and (ii) the presence of a broad peak and no small angle increase in the solution with 1.5 mol·L^{-1} of DEHBA, which is consistent with the predominance of a higher number of smaller aggregates interacting in this solution.

These results are summarized in the MD simulations snapshots represented on Fig 9, where monometallic complexes are highlighted in blue and polymetallic aggregates in green. It shows that the number of polymetallic aggregates increase with the uranyl concentration for the two simulations with [DEHBA] = 0.5 mol·L^{-1}, and that the monometallic $UO_2(NO_3)_2L_2$ complex is clearly the major species for [DEHBA] = 1.5 mol·L^{-1}. Some characteristic aggregates and complexes are reported on Fig 10.

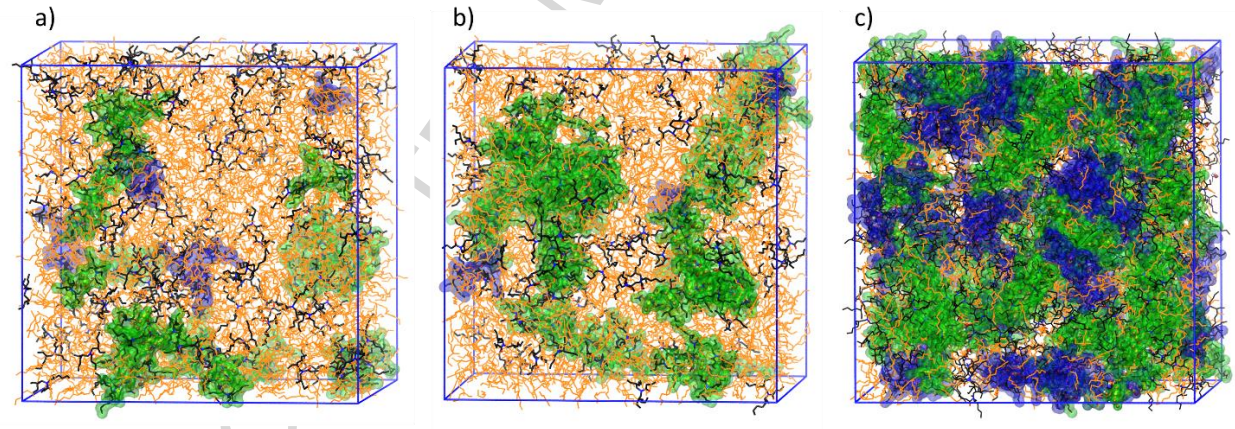

Fig 9 *Snapshots of simulations boxes of DEHBA solution, a) DEHBA 0.5 mol·L^{-1} – U 0.12 mol·L^{-1}, b) DEHBA 0.5 mol·L^{-1} – U 0.22 mol·L^{-1} and c) DEHBA 1.5 mol·L^{-1} – U 0.40 mol·L^{-1}.* Heptane is in orange, carbon in black, nitrogen in blue and oxygen in red. Monometallic complexes are highlighted in blue and polymetallic complexes are highlighted in green.

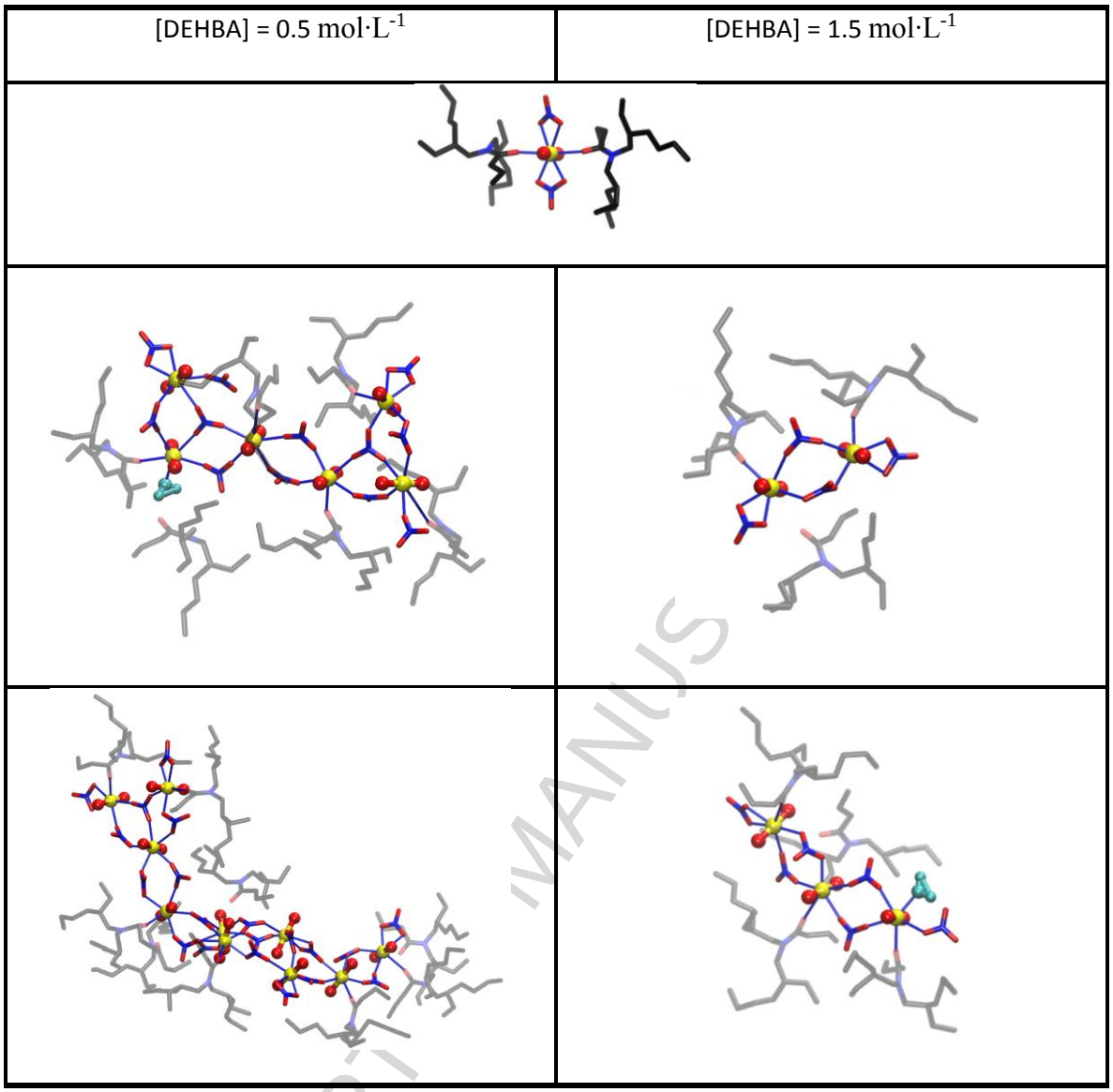

Fig 10 : Representative structures observed in the simulation boxes of DEHBA solutions after extraction of uranyl nitrate. Uranium is yellow, nitrogen is blue, oxygen is red and carbon is black. Hydrogens of DEHBA are not represented. Straight blue lines represent interactions between oxygen and uranium. For a better visibility, DEHBA in aggregates are slightly transparent

Concerning MOEHA, the number of uranium within 6.2 Å of each uranium was calculated. The results show that in the two simulated solutions with [MOEHA] = 0.5 mol·L^{-1}, there are mostly polymetallic aggregates (Table 7) with speciation and organization of the organic phases very similar to what was described for DEHBA. More than 85% of uranyl cations are involved in these aggregates and their proportion increases when the concentration of uranium increases from 0.15 to 0.19 mol·L^{-1}. Similarly to what was observed for DEHBA solutions, nitrates are essentially bridging uranyl cations, and the amount of amide in the first coordination sphere of

uranium is low. Aggregates formed with MOEHA are slightly bigger than the ones formed with DEHBA.

For [MOEHA] = 1.5 mol·L^{-1}, the speciation is truly different compared to the speciation in the concentrated [DEHBA] organic phase. Indeed, the polymetallic species remains the majority, with uranium mainly connected to only one other uranium atom (52%) or to two other uranium atoms (23% involved in larger aggregates). Only 22% of the uranyl cations are involved in the monometallic $UO_2(NO_3)_2L_2$ complex. These results can be seen in both Fig 11 and Fig 12.

This speciation is also consistent with the experimental SWAXS intensities that show more intense low-q scattering upturns for the two solutions with [MOEHA] = 0.5 mol·L^{-1}. There is also a less pronounced broad peak scattering in the intermediate scattering range for the concentrated MOEHA solutions indicating a reduction of the correlation between the aggregates due to a slightly lower aggregate density.

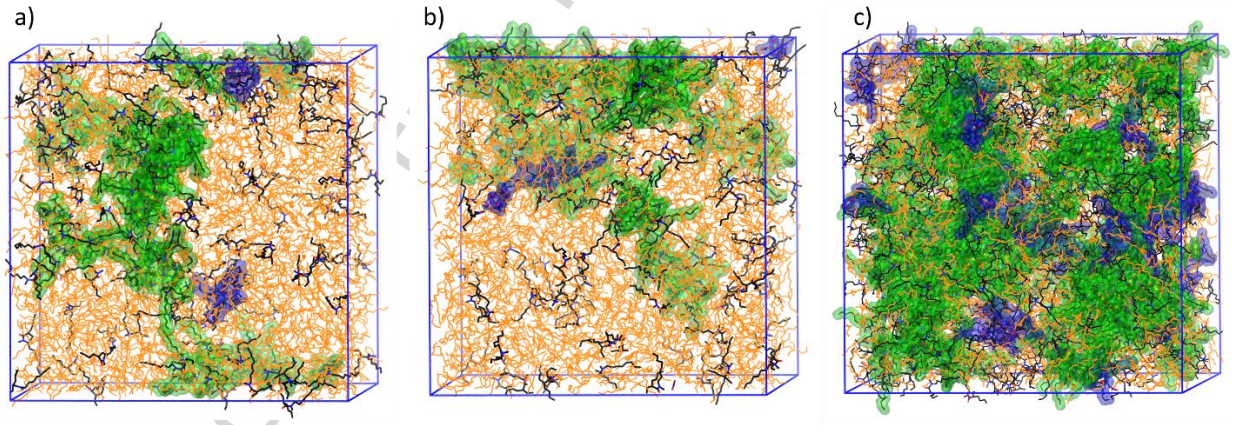

Fig 11 : Snapshots of simulations boxes of MOEHA solution, a) MOEHA 0.5 mol·L^{-1} – U 0.15 mol·L^{-1}, b) MOEHA 0.5 mol·L^{-1} – U 0.19 mol·L^{-1} and c) MOEHA 1.5 mol·L^{-1} – U 0.44 mol·L^{-1}. Heptane is in orange, carbon in black, nitrogen in blue and oxygen in red. Complexes and aggregates of uranyl nitrate are highlighted in blue.

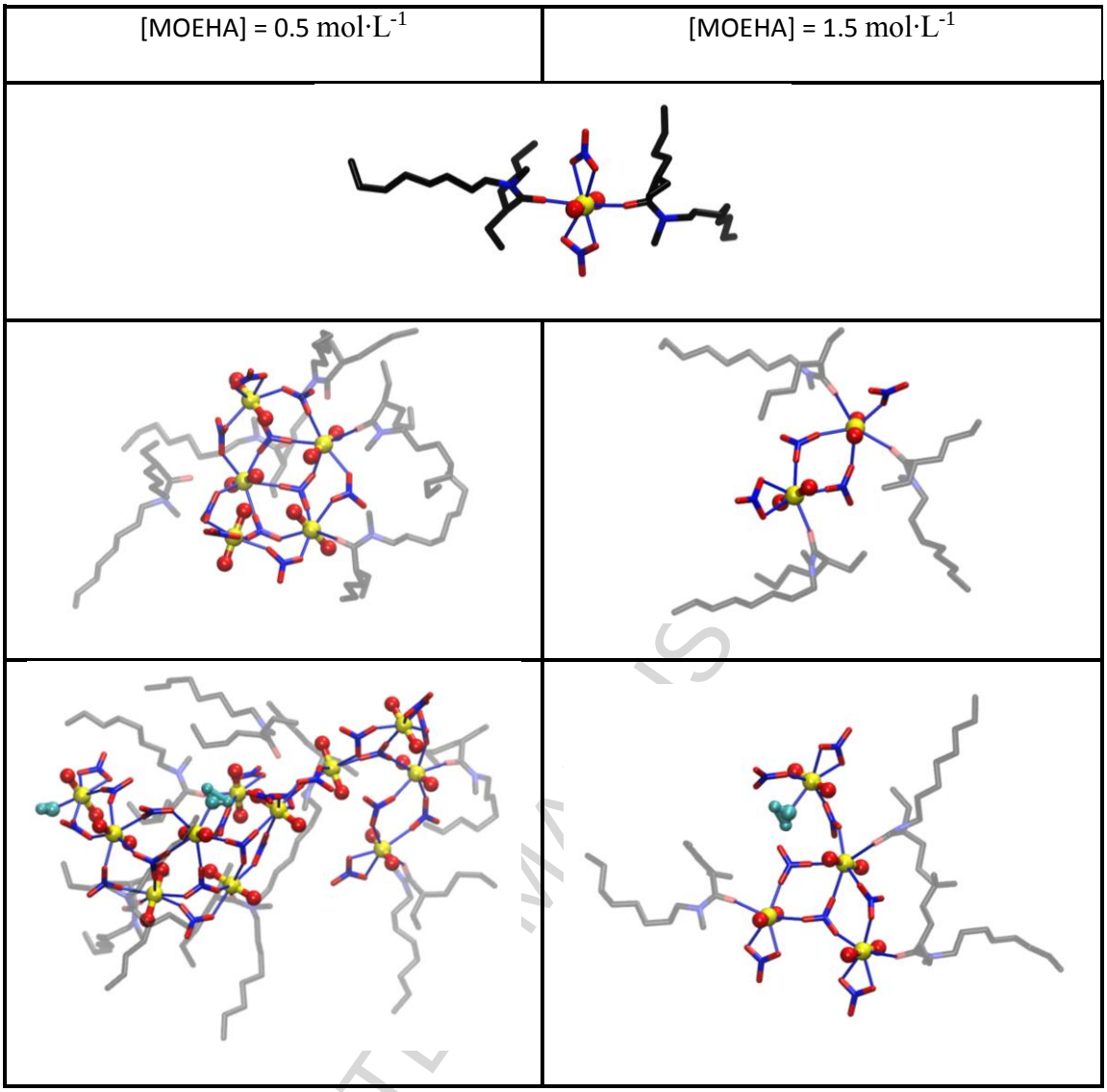

Fig 12 : Representative structures observed in the simulations boxes of MOEHA solutions after extraction of uranyl nitrate. Uranium is yellow, nitrogen is blue, oxygen in red, carbon is black. Hydrogens of DEHBA are not represented. Straight blue lines represent interactions between oxygen and uranium. For a better visibility DEHBA in aggregates are slightly transparent

4. CONCLUSION

This work aimed to characterize the solution organization using two different monoamides in *n*-heptane after water or uranyl nitrate extraction. Some significant differences induced by the structure difference between monoamides are highlighted. Firstly, after water extraction, DEHBA solutions are composed of monomers and dimers which are formed by dipole-dipole interactions or by hydrogen bonds through water molecules. Concerning MOEHA solutions, a higher organization of the solutions is observed with aggregates from 2 to 5 extractant molecules surrounding several water molecules. The higher quantity of water extracted into

MOEHA solutions can be explained by a stronger interaction between extractant molecules that is mediated by water, without the formation of dense, globular inverted structures as seen in the malonamide systems. These results show a correlation between the aggregation and the sterical hindrance on amide function. Indeed, aggregation in the solution decreases with the increase of the steric hindrance in the order MOEHA > DEHBA > DEHiBA. Moreover, water extraction is dependent on the organization of the solution and the amount of water extracted in the organic phases follows the same order as above. This kind of dependency was already observed in other extractant system using TBP or malonamides [28, 43].

Secondly, after uranyl nitrate extraction, solutions at 0.5 mol·L^{-1} of DEHBA are composed of large, dense aggregates of uranyl cations linked together by bridging nitrates. The $UO_2(NO_3)_2L_2$ complex described in the literature is present but only in a small amount. The increase in uranyl concentration leads to an increase of the organization with the formation of more and bigger aggregates. On the contrary, in the solution of 1.5 mol·L^{-1} DEHBA, the $UO_2(NO_3)_2L_2$ complex is the major species and aggregate sizes are smaller. In the case of MOEHA, solutions at 0.5 mol·L^{-1} have a similar organization as the solution of DEHBA at the same concentration, but with larger aggregates and less monometallic complexes. On the other hand, in the solution at 1.5 mol·L^{-1}, even if the proportion of $UO_2(NO_3)_2L_2$ complex increases, the polymetallic aggregates remain the predominant species.

One explanation for this change in organization with the increase of extractant concentration is that at low concentrations (0.5 mol·L^{-1} in *n*-heptane) the medium is essentially non-polar and polar species are concentrated in some areas of the boxes, leading to the formation of large species. In the box at 1.5 mol·L^{-1} of extractant (approximately 2 heptanes for one extractant) the medium is much less non-polar and polar species are no longer trending to aggregates in order to stay in the polar region, species are more regularly spread over the box leading to a decrease in aggregate size.

The organization of these N,N-dialkylamide solutions in *n*-heptane is quite different from the organization of TBP or malonamides solutions [27-29, 43]. After water extraction, organic solutions of TBP or malonamides are organized into small aggregates composed of two to four molecules. After uranyl nitrate extraction by TBP in alkane, polymetallic aggregates containing only 2 to 4 uranyl cations are observed whereas larger polymetallic aggregates are formed in monoamide solutions. This difference of supramolecular organization could explain the different physico-chemical behavior between monoamide and TBP solutions, where for a given concentration of uranyl nitrate, viscosity of the monoamide solutions is higher (exponentially increased) than that of the TBP solutions (linearly increased) [54].

This work could be completed on both the experimental and the MD simulation sides: the nature of the aggregates could be investigated by complementary experimental techniques such as vapor pressure osmometry (VPO) or electrospray ionization mass spectrometry (ESI-MS); and the MD simulations could be analyzed more accurately using a clustering analysis algorithm such as the one used by Shimizu, Bernardes, Lopes et.al. for the structural and aggregation studies in ionic liquids [55-58]. Complementary studies can also be performed for the extraction of uranyl nitrate by the malonamide DMDOHEMA (in order to assess the influence of two amide functions). Moreover, in solvent extraction systems, it is well known that an increase of the solute concentration can lead to third phase formation, the splitting of the organic phase into a light phase composed mostly of the diluent and a heavy third phase containing highly concentrated extractant and ionic solutes [59]. In order to better understand the mechanism responsible for the splitting of the organic phase, this work will also be extended to the characterization of a third phase after uranyl nitrate extraction with N,N-dialkylamide.

ACKNOWLEDGEMENTS

The authors thank ORANO and EDF for financial support and Dr. Ashleigh Kimberlin for her fruitful comments and advices.

SUPPLEMENTARY DATA

Supplementary data to this article can be found online at *XXX*

REFERENCES

[1] T.H. Siddall, Effects of Structure of N,N-Disubstituted Amides on Their Extraction of Actinide and Zirconium Nitrates and of Nitric Acid, J. Phys. Chem., 64 (1960) 1863-1866.
[2] G.M. Gasparini, G. Grossi, Review Article Long Chain Disubstituted Aliphatic Amides as Extracting Agents in Industrial Applications of Solvent Extraction, Solvent Extraction and Ion Exchange, 4 (1986) 1233-1271.
[3] J.N. Mathur, P.B. Ruikar, M.V.B. Krishna, M.S. Murali, M.S. Nagar, R.H. Iyer, Extraction of Np(IV), Np(VI), Pu(IV) and U(VI) with Amides, Behso and Cmpo from Nitric Acid Medium, Radiochim. Acta, 73 (1996) 199-206.
[4] G.M. Gasparini, G. Grossi, Application of N,N-Dialkyl Aliphatic Amides in the Separation of Some Actinides, Sep. Sci. Technol., 15 (1980) 825-844.
[5] C. Musikas, Potentiality of Nonorganophosphorus Extractants in Chemical Separations of Actinides, Sep. Sci. Technol., 23 (1988) 1211-1226.
[6] K.J. Parikh, P.N. Pathak, S.K. Misra, S.C. Tripathi, A. Dakshinamoorthy, V.K. Manchanda, Radiolytic Degradation Studies on N,N-Dihexyloctanamide (DHOA) under Purex Process Conditions, Solvent Extraction and Ion Exchange, 27 (2009) 244-257.
[7] J. Drader, G. Saint-Louis, J.M. Muller, M.C. Charbonnel, P. Guilbaud, L. Berthon, K.M. Roscioli-Johnson, C.A. Zarzana, C. Rae, G.S. Groenewold, B.J. Mincher, S.P. Mezyk, K. McCann, S.G. Boyes, J. Braley, Radiation Chemistry of the Branched-Chain Monoamide Di-2-Ethylhexyl-Isobutyramide, Solvent Extraction and Ion Exchange, 35 (2017) 480-495.
[8] J.A. Drader, N. Boubals, B. Cames, D. Guillaumont, P. Guilbaud, G. Saint-Louis, L. Berthon, Radiolytic Stability of N, N-Dialkyl Amide: Effect on Pu(IV) Complexes in Solution, Dalton Trans., 47 (2018) 251-263.
[9] G. Thiollet, C. Musikas, Synthesis and Uses of the Amides Extractants, Solvent Extraction and Ion Exchange, 7 (1989) 813-827.
[10] G.M. Nair, D.R. Prabhu, G.R. Mahajan, Extraction of Uranium(VI) and Plutonium(IV) with Dihexylbutyramide and Dihexylisobutyramide from Nitric-Acid Medium, J. Radioanal. Nucl. Chem.-Artic., 182 (1994) 393-399.
[11] P.N. Pathak, L.B. Kumbhare, V.K. Manchanda, Effect of Structure of N,N Dialkyl Amides on the Extraction of U(VI) and Th(IV): A Thermodynamic Study, Radiochim. Acta, 89 (2001) 447-452.
[12] D.R. Prabhu, G.R. Mahajan, G.M. Nair, Di(2-Ethyl Hexyl)Butyramide and Di(2-Ethyl Hexyl)Isobutyramide as Extractants for Uranium(VI) and Plutonium(IV), J. Radioanal. Nucl. Chem., 224 (1997) 113-117.
[13] D.R. Prabhu, G.R. Mahajan, G.M. Nair, M.S. Subramanian, Extraction of Uranium(VI) and Plutonium(IV) with Unsymmetrical Monoamides, Radiochim. Acta, 60 (1993) 109-113.
[14] P.N. Pathak, N,N-Dialkyl Amides as Extractants for Spent Fuel Reprocessing: An Overview, J. Radioanal. Nucl. Chem., 300 (2014) 7-15.
[15] N. Condamines, C. Musikas, The Extraction by N.N-Dialkylamides. Ii. Extraction of Actinide Cations, Solvent Extraction and Ion Exchange, 10 (1992) 69-100.
[16] G.M. Nair, G.R. Mahajan, D.R. Prabhu, Extraction of Uranium(VI) and Plutonium(IV) with Some High-Molecular-Weight Aliphatic Monoamides from Nitric-Acid Medium, J. Radioanal. Nucl. Chem.-Artic., 191 (1995) 323-330.
[17] G.M. Nair, G.R. Mahajan, D.R. Prabhu, Dioctyl Butyramide and Dioctyl Isobutyramide as Extractants for Uranium(VI) and Plutonium(IV), J. Radioanal. Nucl. Chem.-Artic., 204 (1996) 103-111.

[18] N. Tsutsui, Y. Ban, H. Sagawa, S. Ishii, T. Matsumura, Solvent Extraction of Uranium with N,N-Di(2-Ethylhexyl)Octanamide from Nitric Acid Medium, Solvent Extraction and Ion Exchange, 35 (2017) 439-449.
[19] V.K. Manchanda, P.B. Ruikar, S. Sriram, M.S. Nagar, P.N. Pathak, K.K. Gupta, R.K. Singh, R.R. Chitnis, P.S. Dhami, A. Ramanujam, Distribution Behavior of U(VI), Pu(IV), Am(III), and Zr(IV) with N,N-Dihexyl Octanamide under Uranium-Loading Conditions, Nuclear Technology, 134 (2001) 231-240.
[20] K. McCann, J.A. Drader, J.C. Braley, Comparing Branched Versus Straight-Chained Monoamide Extractants for Actinide Recovery, Separation & Purification Reviews, 47 (2018) 49-65.
[21] P.K. Verma, P.K. Mohapatra, A. Bhattacharyya, A.K. Yadav, S.N. Jha, D. Bhattacharyya, Structural Investigations on Uranium(VI) and Thorium(IV) Complexation with Tbp and Dhoa: A Spectroscopic Study, New Journal of Chemistry, 42 (2018) 5243-5255.
[22] P. Charpin, M. Lance, M. Nierlich, D. Vigner, J. Livet, C. Musikas, Structures of Uranyl and Tetraalkylammonium Azide Complexes .1. Uranyl and Tetraethylammonium Triazides .2. Uranyl and Tetramethylammonium Mu-3-Oxoazides, Acta Crystallogr. Sect. C-Cryst. Struct. Commun., 42 (1986) 1691-1694.
[23] E. Acher, Y.H. Cherkaski, T. Dumas, C. Tamain, D. Guillaumont, N. Boubals, G. Javierre, C. Hennig, P.L. Solar, M.C. Charbonnel, Structures of Plutonium(IV) and Uranium(VI) with N,N-Dialkyl Amides from Crystallography, X-Ray Absorption Spectra, and Theoretical Calculations, Inorg. Chem., 55 (2016) 5558-5569.
[24] G. Ferru, L. Berthon, C. Sorel, O. Diat, P. Bauduin, J.P. Simonin, Influence of Extracted Solute on the Organization of a Monoamide Organic Solution, Procedia Chemistry, 7 (2012) 27-32.
[25] P.K. Verma, N. Kumari, P.N. Pathak, B. Sadhu, M. Sundararajan, V.K. Aswal, P.K. Mohapatra, Investigations on Preferential Pu(IV) Extraction over U(VI) by N,N-Dihexyloctanamide Versus Tri-N-Butyl Phosphate: Evidence through Small Angle Neutron Scattering and Dft Studies, Journal of Physical Chemistry A, 118 (2014) 3996-4004.
[26] F. Rodrigues, G. Ferru, L. Berthon, N. Boubals, P. Guilbaud, C. Sorel, O. Diat, P. Bauduin, J.P. Simonin, J.P. Morel, N. Morel-Desrosiers, M.C. Charbonnel, New Insights into the Extraction of Uranium(VI) by an N,N-Dialkylamide, Molecular Physics, 112 (2014) 1362-1374.
[27] G. Ferru, D. Gomes Rodrigues, L. Berthon, O. Diat, P. Bauduin, P. Guilbaud, Elucidation of the Structure of Organic Solutions in Solvent Extraction by Combining Molecular Dynamics and X-Ray Scattering, Angewandte Chemie, 53 (2014) 5346-5350.
[28] P. Guilbaud, L. Berthon, W. Louisfrema, O. Diat, N. Zorz, Determination of the Structures of Uranyl-Tri-N-Butyl-Phosphate Aggregates by Coupling Experimental Results with Molecular Dynamic Simulations, Chem.-Eur. J., 23 (2017) 16660-16670.
[29] A.G. Baldwin, Y. Yang, N.J. Bridges, J.C. Braley, Tributyl Phosphate Aggregation in the Presence of Metals: An Assessment Using Diffusion Nmr Spectroscopy, The Journal of Physical Chemistry B, 120 (2016) 12184-12192.
[30] L. Martinez, R. Andrade, E.G. Birgin, J.M. Martinez, Packmol: A Package for Building Initial Configurations for Molecular Dynamics Simulations, J. Comput. Chem., 30 (2009) 2157-2164.
[31] V.B. D.A. Case, J.T. Berryman, R.M. Betz, Q. Cai, D.S. Cerutti, T.E. Cheatham, III, T.A. Darden, R.E., H.G. Duke, A.W. Goetz, S. Gusarov, N. Homeyer, P. Janowski, J. Kaus, I. Kolossváry, A. Kovalenko,, S.L. T.S. Lee, T. Luchko, R. Luo, B. Madej, K.M. Merz, F. Paesani, D.R. Roe, A. Roitberg, C. Sagui,, G.S. R. Salomon-Ferrer, C.L. Simmerling, W. Smith, J. Swails, R.C. Walker, J. Wang, R.M. Wolf, X., W.a.P.A. Kollman, Amber 14, University of California, San Francisco, 2014.
[32] W.D. Cornell, P. Cieplak, C.I. Bayly, I.R. Gould, K.M. Merz, D.M. Ferguson, D.C. Spellmeyer, T. Fox, J.W. Caldwell, P.A. Kollman, A 2nd Generation Force-Field for the Simulation of Proteins, Nucleic-Acids, and Organic-Molecules, J. Am. Chem. Soc., 117 (1995) 5179-5197.
[33] D.A. Case, T.E. Cheatham, T. Darden, H. Gohlke, R. Luo, K.M. Merz, A. Onufriev, C. Simmerling, B. Wang, R.J. Woods, The Amber Biomolecular Simulation Programs, J. Comput. Chem., 26 (2005) 1668-1688.
[34] W. Kunz, L. Belloni, O. Bernard, B.W. Ninham, Osmotic Coefficients and Surface Tensions of Aqueous Electrolyte Solutions: Role of Dispersion Forces, J. Phys. Chem. B, 108 (2004) 2398-2404.

[35] T. Fox, P.A. Kollman, Application of the Resp Methodology in the Parametrization of Organic Solvents, J. Phys. Chem. B, 102 (1998) 8070-8079.
[36] C.I. Bayly, P. Cieplak, W.D. Cornell, P.A. Kollman, A Well-Behaved Electrostatic Potential Based Method Using Charge Restraints for Deriving Atomic Charges - the Resp Model, J. Phys. Chem., 97 (1993) 10269-10280.
[37] E.C. Meng, P.A. Kollman, Molecular Dynamics Studies of the Properties of Water around Simple Organic Solutes, J. Phys. Chem., 100 (1996) 11460-11470.
[38] T.N. Nguyen, M. Duvail, A. Villard, J.J. Molina, P. Guilbaud, J.F. Dufreche, Multi-Scale Modelling of Uranyl Chloride Solutions, J. Chem. Phys., 142 (2015) 11.
[39] T. Darden, D. York, L. Pedersen, Particle Mesh Ewald - an N.Log(N) Method for Ewald Sums in Large Systems, J. Chem. Phys., 98 (1993) 10089-10092.
[40] W. Humphrey, A. Dalke, K. Schulten, Vmd: Visual Molecular Dynamics, J. Mol. Graph., 14 (1996) 33-38.
[41] T. Rog, K. Murzyn, K. Hinsen, G.R. Kneller, Nmoldyn: A Program Package for a Neutron Scattering Oriented Analysis of Molecular Dynamics Simulations, J. Comput. Chem., 24 (2003) 657-667.
[42] C. Erlinger, D. Gazeau, T. Zemb, C. Madic, L. Lefrançois, M. Hebrant, C. Tondre, Effect of Nitric Acid Extraction on Phase Behavior, Microstructure and Interactions between Primary Aggregates in the System Dimethyldibutyltetradecylmalonamide (DMDBTDMA) / N-Dodecane / Water: A Phase Analysis and Small Angle X-Ray Scattering (SAXS) Characterisation Study, Solvent Extraction and Ion Exchange, 16 (1998) 707-738.
[43] Y. Meridiano, L. Berthon, X. Crozes, C. Sorel, P. Dannus, M.R. Antonio, R. Chiarizia, T. Zemb, Aggregation in Organic Solutions of Malonamides: Consequences for Water Extraction, Solvent Extraction and Ion Exchange, 27 (2009) 607-637.
[44] Q.N. Vo, L.X. Dang, M. Nilsson, H.D. Nguyen, Quantifying Dimer and Trimer Formation by Tri-N-Butyl Phosphates in N-Dodecane: Molecular Dynamics Simulations, J. Phys. Chem. B, 120 (2016) 6985-6994.
[45] Q.N. Vo, J.L. Unangst, H.D. Nguyen, M. Nilsson, Quantifying Dimer and Trimer Formation of Tri-N-Butyl Phosphates in Different Alkane Diluents: Ftir Study, J. Phys. Chem. B, 120 (2016) 6976-6984.
[46] R. Motokawa, S. Suzuki, H. Ogawa, M.R. Antonio, T. Yaita, Microscopic Structures of Tri-N-Butyl Phosphate/N-Octane Mixtures by X-Ray and Neutron Scattering in a Wide Q Range, J. Phys. Chem. B, 116 (2012) 1319-1327.
[47] T.L. Greaves, A. Weerawardena, C.J. Drummond, Nanostructure and Amphiphile Self-Assembly in Polar Molecular Solvents: Amides and the “Solvophobic Effect”, Physical Chemistry Chemical Physics, 13 (2011) 9180-9186.
[48] L. Berthon, L. Martinet, F. Testard, C. Madic, T. Zemb, Solvent Penetration and Sterical Stabilization of Reverse Aggregates Based on the Diamex Process Extracting Molecules: Consequences for the Third Phase Formation, Solvent Extraction and Ion Exchange, 25 (2007) 545-576.
[49] F. Testard, P. Bauduin, L. Martinet, B. Abécassis, L. Berthon, C. Madic, T. Zemb, Self-Assembling Properties of Malonamide Extractants Used in Separation Processes, Radiochim. Acta, 96 (2008).
[50] L. Berthon, F. Testard, L. Martinet, T. Zemb, C. Madic, Influence of the Extracted Solute on the Aggregation of Malonamide Extractant in Organic Phases: Consequences for Phase Stability, C. R. Chim., 13 (2010) 1326-1334.
[51] R.J. Ellis, Y. Meridiano, J. Muller, L. Berthon, P. Guilbaud, N. Zorz, M.R. Antonio, T. Demars, T. Zemb, Complexation-Induced Supramolecular Assembly Drives Metal-Ion Extraction, Chemistry, 20 (2014) 12796-12807.
[52] C. Déjugnat, L. Berthon, V. Dubois, Y. Meridiano, S. Dourdain, D. Guillaumont, S. Pellet-Rostaing, T. Zemb, Liquid-Liquid Extraction of Acids and Water by a Malonamide: I-Anion Specific Effects on the Polar Core Microstructure of the Aggregated Malonamide, Solvent Extraction and Ion Exchange, 32 (2014) 601-619.

[53] M.R. Antonio, R. Chiarizia, B. Gannaz, L. Berthon, N. Zorz, C. Hill, G. Cote, Aggregation in Solvent Extraction Systems Containing a Malonamide, a Dialkylphosphoric Acid and Their Mixtures, Sep. Sci. Technol., 43 (2008) 2572-2605.
[54] P.N. Pathak, A.S. Kanekar, D.R. Prabhu, V.K. Manchanda, Comparison of Hydrometallurgical Parameters of N,N-Dialkylamides and of Tri-N-Butylphosphate, Solvent Extraction and Ion Exchange, 27 (2009) 683-694.
[55] C.E.S. Bernardes, M.E.M. da Piedade, J.N.C. Lopes, The Structure of Aqueous Solutions of a Hydrophilic Ionic Liquid: The Full Concentration Range of 1-Ethyl-3-Methylinnidazolium Ethylsulfate and Water, J. Phys. Chem. B, 115 (2011) 2067-2074.
[56] C.E.S. Bernardes, K. Shimizu, A.I.M.C.L. Ferreira, L.M.N.B.F. Santos, J.N.C. Lopes, Structure and Aggregation in the 1,3-Dialkyl-Imidazolium Bis(Trifluoromethylsulfonyl)Imide Ionic Liquid Family: 2. From Single to Double Long Alkyl Side Chains, J. Phys. Chem. B, 118 (2014) 6885-6895.
[57] D.W. Bruce, C.P. Cabry, J.N.C. Lopes, M.L. Costen, L. D'Andrea, I. Grillo, B.C. Marshall, K.G. McKendrick, T.K. Minton, S.M. Purcell, S. Rogers, J.M. Slattery, K. Shimizu, E. Smoll, M.A. Tesa-Serrate, Nanosegregation and Structuring in the Bulk and at the Surface of Ionic-Liquid Mixtures, J. Phys. Chem. B, 121 (2017) 6002-6020.
[58] K. Shimizu, C.E.S. Bernardes, J.N.C. Lopes, Structure and Aggregation in the 1-Alkyl-3-Methylimidazolium Bis(Trifluoromethylsulfonyl)Imide Ionic Liquid Homologous Series, J. Phys. Chem. B, 118 (2014) 567-576.
[59] P.B. F. Testard, T. Zemb, and L. Berthon, Third-Phase Formation in Liquid/Liquid Extraction: A Colloidal Approach, CRC Press, Taylor and Francis Group2009.

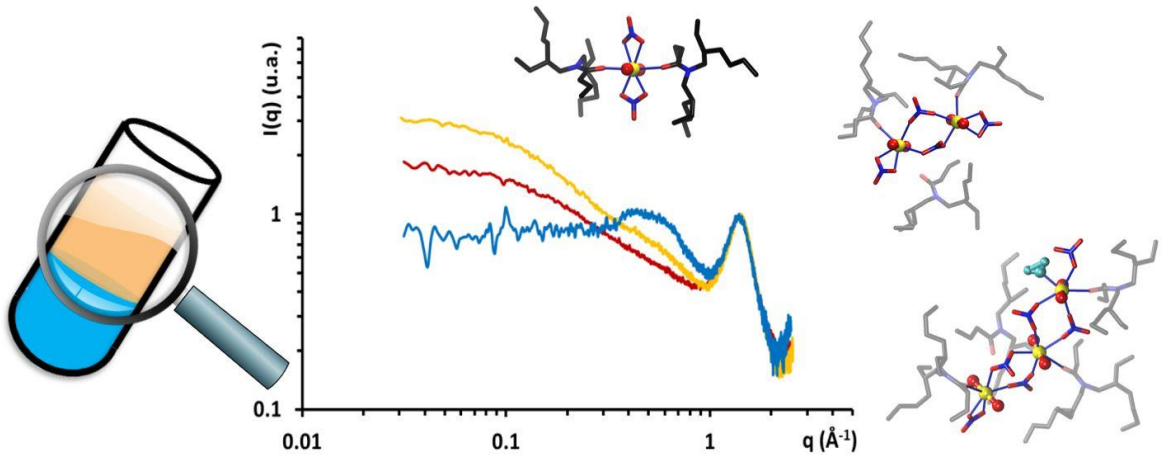

Graphical abstract

Highlights

- Coupling SWAXS and MD simulations lead to a better speciation in organic phases
- Small aggregates are formed with monoamides after extraction of water molecules
- Solvent extraction of uranyl nitrate lead to polynuclear aggregation in the organic phases
- The speciation and the aggregation depends on the ramification on the monoamide
- Aggregation may be more important at lower extractant concentration